IOP Publishing Journal of Micromechanics and Microengineering
J. Micromech. Microeng. **26** (2016) 115013 (10pp) doi:10.1088/0960-1317/26/11/115013

Comparative analysis of fabrication methods for achieving rounded microchannels in PDMS

Nicholas W Bartlett[1,2] **and Robert J Wood**[1,2]

[1] John A Paulson School of Engineering and Applied Sciences, Harvard University, Cambridge, MA, USA
[2] Wyss Institute for Biologically Inspired Engineering, Harvard University, Cambridge, MA, USA

E-mail: nbartlett@seas.harvard.edu

Received 28 June 2016, revised 1 September 2016
Accepted for publication 20 September 2016
Published 7 October 2016

Abstract

Many microfluidic applications demand control over channel cross-sectional geometry. In particular, rounded microchannels are essential to the function of microfluidic valves, which have played an integral part in the success of microfluidics over the past fifteen years. Here we investigate the relative strengths and weaknesses of different strategies for fabricating rounded microchannels in PDMS, systematically examining five common strategies. We consider the appropriateness of the fabrication strategies for microchannels of differing sizes and aspect ratios, and evaluate these various strategies on a number of metrics ranging from microchannel resolution to fabrication difficulty. We discuss the merits of the different strategies for a range of applications, and make recommendations on which strategy to use based on the driving constraints of the device.

Keywords: microfludics, PDMS, microchannel shape, microvalve, fabrication, soft lithography, 3D printing

S Online supplementary data available from stacks.iop.org/JMM/26/115013/mmedia

(Some figures may appear in colour only in the online journal)

Introduction

In microfluidics, standard photolithographic techniques produce vertical sidewalls, yielding channels with rectangular cross sections. Such microchannels may be appropriate for a number of applications, but they pose extreme challenges in other areas, such as modeling vascular networks [1–3] and optofluidics [4–6], to name just a few examples. Consequently, one often wants control over the cross-sectional geometry of the microchannel.

Channel shape is perhaps most critical in the case of microfluidic valves. Given two perpendicularly oriented microchannels that are slightly offset in the vertical dimension (so that only a thin membrane separates them), pressurizing one channel causes a deflection of the membrane into the second channel such that flow in the second channel is impeded (see figure 1). In this way, the flow within a microchannel can be modulated by the flow within a different, independent microchannel. First reported in 2000 by Unger *et al* [7], microfluidic valves enable interactions between two disconnected microchannels. In that work, the authors demonstrate the capabilities of their valve by creating an elastomeric peristaltic pump. In 2002, Thorsen *et al* [8] expanded this work to address large-scale integration, opening the doors to microfluidic multiplexors in which thousands of microchannels can be controlled with only a few inputs. Later work also looked at using these valves to make other pumps [9] and mixers [10]. Additionally, microfluidic valves have become integral in biological automation [11], cell sorting [12], and protein separation [13]. They have been used to perform multiplexing [14] and, more recently, in digital fluidic logic, creating complex devices such as oscillators and shift registers [15].

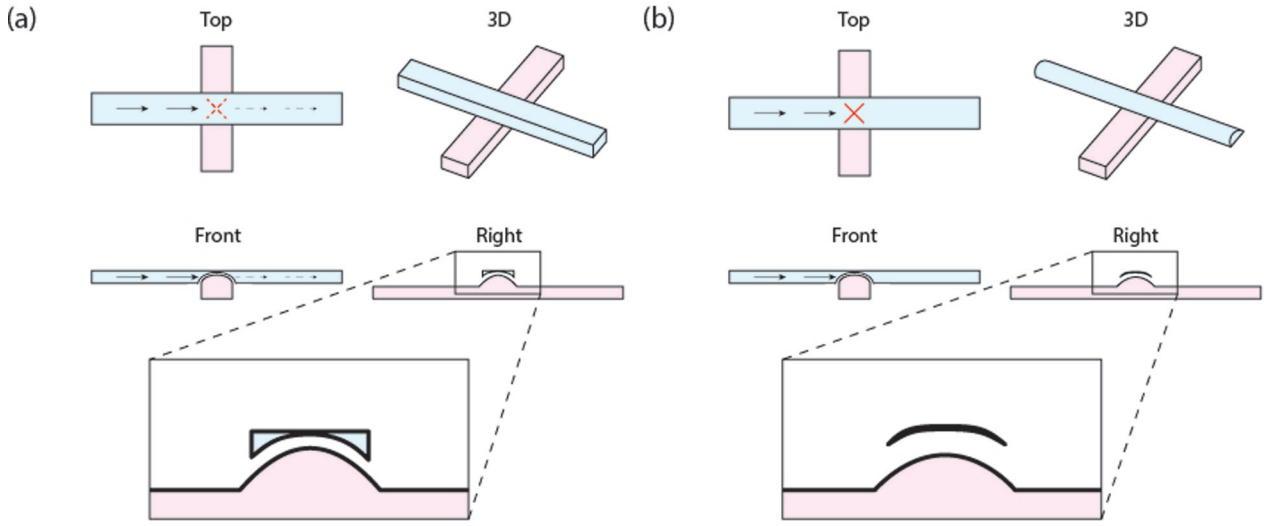

Figure 1. Sketches of the operation of a microfluidic valve with (a) rectangular microchannels and (b) rounded microchannels. The control channel (red) is pressurized, which deflects the membrane and closes the flow channel (blue). Flow in (a) the rectangular microchannel is only partially stopped, while in (b) the rounded microchannel it is completely stopped.

There are a number of important parameters in the design of an effective microfluidic valve. As discussed in Studer *et al* [16], membrane thickness, whether the valve is push-up or push-down, channel aspect ratio, and general scaling properties are all crucial considerations. But most fundamental to the basic functionality of a microfluidic valve is the channel profile. If a microchannel has a rectangular cross section, the deflected membrane cannot fully collapse into the sharp corners, and flow will not be stopped. A number of groups have looked at modeling valve closure mechanics, and have identified the most promising cross-sectional geometries [7, 17–21]. These papers unanimously agree that a channel with rounded corners is necessary for complete valve closure. The difference in valve operation between rectangular microchannels and rounded microchannels can be seen in figure 1.

Previous studies have already identified and analyzed the ideal channel shape; in this work, we are interested in the fabrication strategies that best produce that shape. In that regard, a number of techniques have been proposed. The first microfluidic valves were fabricated by molding off of masters that were made with a positive photoresist. When heated to an elevated temperature, the positive photoresist reflows, creating rounded features [7]. This technique has been adopted by a number of later groups [22–24], and has garnered enough attention to merit a systematic characterization of the method [18]. However, there are a number of challenges associated with this method, such as the relatively low chemical and thermal stability of many positive photoresists compared to more robust alternatives [25, 26]. Particularly, some of the most common positive photoresists (e.g. SPR 220) fail to integrate well with some of the most common negative photoresists (e.g. SU-8), so even using positive photoresists only for the valves becomes impractical [27]. Consequently, researchers have investigated alternative fabrication strategies. 3D printing microfluidic molds was first suggested long ago [28], and now researchers are directly printings microfluidic networks [29]; a recent review presents an updated analysis of this fabrication technique [30]. Some researchers have created rounded microchannels by exposing photoresist through the backside of a glass wafer with diffuse light [17], using an inflated PDMS membrane as a mold [21], and spin coating a second layer of photoresist to exploit capillarity [27]. Yet others have relied on gray-scale photolithography [31–34], the surface tension of PDMS [35, 36], laser micromachining [37], removal of a cylindrical element [38–43], femtosecond laser pulses [5, 6] and more.

In this paper we examine in detail five techniques most applicable to the fabrication of microfluidic valves. We do so by fabricating microfluidic channels of the same dimensions with the five different techniques, and systematically catalog the variations. In doing so, we provide a direct comparison between these different techniques. The most important evaluation parameter is whether a given technique is able to achieve a rounded microchannel; we determine the quality of the microchannel shape by building example valves and measuring their performance. After considering the cross-sectional geometry of the channels, we evaluate each fabrication strategy on a number of additional metrics, which are described in the next section.

Design of experiments

The fabrication strategies were evaluated on microfluidic channels of varying dimensions, which can be seen in figure 2. Target channel heights were 10 and 50 μm and target channel widths were 50, 100, and 250 μm, resulting in six distinct channel geometries with aspect ratios ranging from 1:1 to 1:25. (Note that these values intentionally challenge commonly accepted channel aspect ratio limits [44]. We are interested in how the various fabrication strategies perform not only in conservative microfluidic device designs, but in aggressive designs as well.)

For each fabrication strategy, we altered one key parameter to determine the sensitivity of the technique; in particular, we investigated three variations of each strategy. For five fabrication

strategies with three parameter variations and six different channel dimensions, this equates to ninety unique channels to be compared (in addition to the six control channels).

Evaluation of the various fabrication strategies is not limited to the resultant channel cross-sectional geometry (i.e. how well the strategy can produce rounded channels). In addition, we consider resolution (i.e. the size limit of features that can be made), dimension mapping (i.e. the correlation between design dimensions and actual device dimensions), fabrication time (both active and passive), fabrication difficulty (i.e. the amount of skill required and how tightly the process must be controlled), and process prohibitiveness (including such factors as the cost of necessary equipment, and the toxicity of chemicals involved).

Methods

All strategies but one rely at least in part on the soft lithography process [45]. In this process, a poly(dimethylsiloxane) (PDMS) device is molded from a master that is (typically) fabricated using photolithography. To make a master, a photosensitive polymer (i.e. photoresist) is poured onto a substrate (typically a silicon wafer). When spun at high speeds, the photoresist coats the substrate evenly at a controllable thickness. After spin coating, the photoresist is exposed to a UV light source through a photomask, effectively transferring the pattern from the photomask to the photoresist. Upon being placed in a developing solution, the photoresist is selectively removed, leaving only the desired pattern. After surface treatment to prevent sticking, the photolithographic master can now be used to mold PDMS devices that will have the inverse structure of the master.

For each method involving photolithography, we used photomasks that were custom fabricated from a thin (12.7 μm) UV-impenetrable, polyimide film (Kapton, DuPont USA) cut on a diode-pumped solid-state laser (see supplemental information for additional details (stacks.iop.org/JMM/26/115013/mmedia)).

Control

Control devices were fabricated using the standard soft lithography process. Three inch, ⟨1 0 0⟩, virgin test grade, boron doped, p-type silicon wafers (ID:447, University Wafer) were used as the substrate. The 10 μm channels were fabricated with SU-8 2010 (MichroChem Corp.) while the 50 μm channels were fabricated with SU-8 2050 (MichroChem Corp.). Exposure was performed using a MAS 500 IR/VIS Mask Alignment and Exposure system, with a measured exposure power of 21.9 mW cm^{-2} at 365 nm. For development, we used SU-8 Developer (MichroChem Corp.). For surface treatment, the silicon wafers were exposed to silane (trichloro(1H, 1H, 2H, 2H-perfluorooctyl)silane, Sigma-Aldrich) vapor in a dessicator. See supplemental information for details on the exact fabrication parameters.

After silanizing the wafers overnight, we poured PDMS (Sylgard 184, Dow Corning) that had been mixed in a 10:1 ratio (base:curing agent) over the wafers, degassed under vacuum to remove bubbles, and cured. Curing was typically done at 60 °C for at least four hours, although occasionally we cured at higher temperatures (up to 70 °C) for shorter durations to enable faster process iteration.

Once cured, the PDMS was removed from the wafer and manually cut with a razor blade into thin (approximately 2 mm) slices to view the cross section of the channels. We used a confocal microscope (Olympus LEXT OLS4000, Olympus Corporation) to evaluate the channels and take dimensional data, while we used a scanning electron microscope (SEM) to take the images that are presented in this paper.

Except where noted, all of the strategies tested use the same fabrication procedure as has been described for the control devices.

Reflow of positive photresist (+PR)

Perhaps the most common method to achieve rounded microchannels is to reheat a developed photoresist pattern slightly beyond its melting temperature such that the photoresist begins to flow. Surface tension causes the corners of the device to round, changing the cross-sectional geometry of the device to a new shape that is retained upon cooling.

Unfortunately, SU-8 does not melt at a sufficiently low temperature to enable reflow. In the following procedure we used Megaposit SPR 220-7.0 positive photoresist (Dow Chemical Company). First, we prebaked a virgin silicon wafer at 115 °C for five minutes. After cooling back to room temperature, we spincoated hexamethyldisilazane (HMDS) at 2000 rpm to promote adhesion of the photoresist to the wafer. We then spincoated the photoresist at 1500 rpm for a target thickness of 10 μm. We soft baked at 115 °C for 90 s, and exposed at an energy dose of approximately 1300 mJ cm^{-2}. The photoresist was then allowed to rehydrate for at least four hours, after which we performed a post exposure bake at 115 °C for five minutes. After allowing full cooling back to room temperature (at least 20 min), we developed in Megaposit MF-24A Developer (Dow Chemical Company) until the features were appropriately defined (which can take 10–30 min). Once dry, we placed the wafer on a hotplate (set to either 90, 120, or 150 °C) for five minutes to reflow the photoresist. See supplemental information for details on the exact fabrication parameters.

Due to the viscosity of SPR 220-7.0, the maximum thickness of photoresist that can be achieved in a single spincoat is limited. In order to achieve a 50 μm layer of photoresist, multiple spincoat-bake cycles are required. Although multiple spincoat procedures producing layers up to about 54 μm have been reported [46], we found this procedure to be much too sensitive to warrant serious investigation. As such, we were unable to create any 50 μm thick devices using positive photoresist.

3D printing (3DP)

Among the fabrication strategies examined, 3D printing is unique in that it does not involve any type of photolithography.

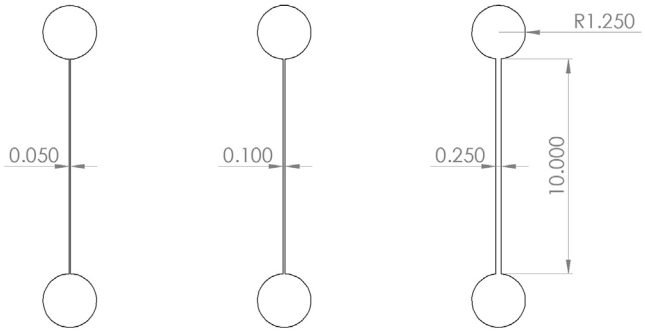

Figure 2. A schematic of the channel dimensions that were used to evaluate the five fabrication strategies. All dimensions are in millimeters. These three channels were fabricated at thicknesses of both 10 and 50 μm.

Molds were designed using commercially available CAD software (Solidworks, Dassault Systemes SOLIDWORKS Corp.).

For this method, we chose three different printers to compare: an Objet30 Scholar (Stratasys Ltd.), a Form 1+ (Formlabs), and a Titan 1 (Kudo3D Inc). The Objet30 uses a technique called PolyJet printing (a form of inkjet printing), in which droplets of liquid photopolymer are jetted onto a build tray, and then flash-cured with a UV light. The Form 1+ operates as a stereolithgraphy (SLA) printer, in which a focused UV laser traces patterns in a vat of liquid photopolymer. The Titan 1, also an SLA printer, is slightly different in that it uses digital light processing (DLP), in which the image of the entire layer is projected at once. We chose not to examine a fused deposition modeling (FDM) 3D printer; although these printers are among the most common style of printers, they often have relatively poor resolution. Conversely, 3D printers that use two-photon polymerization, such as the Nanoscribe (Nanoscribe GmbH), are able to achieve sub-micrometer resolution, but have a significantly limited build volume and are often prohibitively expensive. As such, they are outside the scope of this investigation. A thorough discussion of the various types of 3D printing can be found in a recent review by Waheed *et al* [30].

Backside exposure through glass wafer (BSE)

This fabrication procedure closely follows the one outlined by Futai *et al* [17], although with some minor variations. In this process, we used a 200 μm thick, 100 mm diameter borosilicate glass wafer (V015.04-1004, Plan Optik AG) instead of a silicon wafer as is traditionally used in photolithography. After the soft bake, the wafer is flipped over and the photomask is placed on the backside of the glass wafer. As a result, the photomask is offset from the photoresist by the thickness of the wafer. When the photoresist is exposed with diffuse (rather than collimated) UV light, the photomask offset causes the resulting channels to have sloping rather than vertical sidewalls. Because our UV light source outputs collimated light, we had to introduce an additional optical element. For this modification we placed a 120 grit UV fused silica ground glass diffuser (DGUV10-120, Thorlabs Inc.) approximately 7 mm above the photomask.

The test parameter that we varied in this fabrication strategy was the exposure energy. For both the 10 and 50 μm devices, we chose to expose at the recommended energy (from the datasheet) and at both 50 and 100 mJ cm^{-2} above the recommended value. For the 10 μm device (using SU-8 2010), this corresponds to exposure energies of 125, 175, and 225 mJ cm^{-2}, while for the 50 μm device (using SU-8 2050), this corresponds to 150, 200, and 250 mJ cm^{-2}. Although the exposure power of our UV light source was measured to be 21.9 mW cm^{-2}, the exposure power through the glass wafer was reduced to 20.4 mW cm^{-2}, and further reduced to 12.3 mW cm^{-2} when the diffuser was introduced. Thus, we used this last value (12.3 mW cm^{-2}) when calculating the relevant exposure times.

Inflated PDMS membrane (IPM)

Following the work of Hongbin *et al* [21], this fabrication strategy uses a PDMS device as the mold for a second PDMS device. In this method, the first PDMS device is made using the standard soft lithography process. This PDMS device is then bonded to a thin PDMS layer that has been spun onto a silicon wafer at 1000 rpm, resulting in a membrane that is about 75 μm thick. To bond the two layers, we exposed the PDMS to oxygen plasma (35 W at 0.4 mbar for 20 s) using a low pressure plasma system (Pico BR PCCE 7", Diener electronic GmbH + Co. KG). After silanizing the resultant PDMS device, we had a set of functional microfluidic channels. This device was then used as a mold for the second PDMS device. We punched inlet holes and connected the channels to a pressure-regulated air supply. Pressurizing the channels caused the thin membrane to deflect. We then cast a new layer of PDMS over the PDMS mold (while still under pressure), and cured. In this way, the shape of the deflected membrane of the PDMS mold is transfered to the resulting PDMS device. See Hongbin *et al* [21] for a figure showing this process, and supplemental information for additional fabrication details.

As reported by Hongbin *et al* [21], the deflection of the membrane depends in part on the width of the channel. However, it also depends in part on the degree of pressurization. Thus, we tested this procedure under inflation pressures of 1, 3, and 5 psi (6.89, 20.68 and 34.47 kPa, respectively). These pressures are higher than those reported by Hongbin *et al*, but are reasonable due to the fact that we used a thicker membrane.

Secondary spin coating (SSC)

The final fabrication strategy examined here is based on the 'thin film wings' method reported by Dy *et al* [27]. In this method, a master is made in the typical photolithographic procedure using SU-8 photoresist. As such, the structure will have vertical side walls and sharp corners. A thin film of SU-8 is then spun onto the structure. Capillary action causes the liquid SU-8 to wick into the sharp corners of the master. After

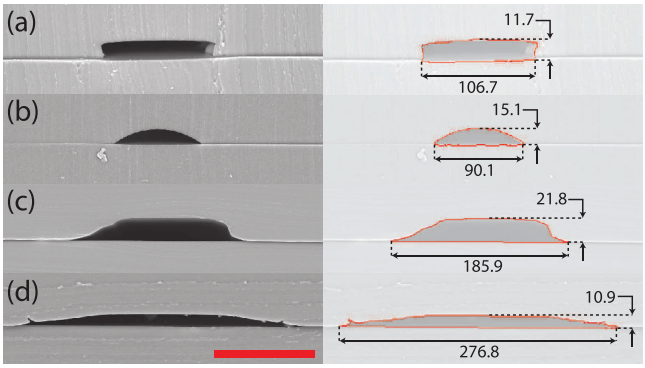

Figure 3. SEM images of 10×100 μm channels for the different techniques. (a) Control. (b) Positive photoresist, reflowed for 5 min at 150 °C. (c) 3D printed mold on Titan 1 from Kudo3D. (d) Backside exposure at 225 mJ cm^{-2} exposure energy. As the last two methods (IPM and SSC) failed to produce channels of the specified dimensions, we do not include them here. (Left) Original SEM image. (Right) SEM image with channel highlighted and dimensions added. All dimensions are in micrometers. Scale bar is 100 μm.

soft bake, exposure, and post exposure bake, the secondary photoresist layer adheres to the original photoresist structure, resulting in a final master that features rounded corners. See supplemental information for details on the exact fabrication parameters.

For this fabrication method, we varied the spin coat speed to control the thickness of the second photoresist layer. We were careful to try to deposit the same amount of photoresist on each sample, which was a roughly 25 mm diameter pool of photoresist in the center of the wafer. The spin coat speeds we tested were 1000, 2000 and 4000 rpm.

Results and discussion

Summary of results

Compared to the control, all of the fabrication techniques produced rounded microchannels, indicating good performance as microfluidic valves. The detailed results for each method will be presented in the following sections as well as in the conclusion; here we compare the results across methods.

In figure 3 we compare the shapes of the channels fabricated from the different techniques. For easy comparison, here we only consider the 10×100 μm channels. Because neither the inflated PDMS method nor the secondary spin coating method produced channels of 10×100 μm, they are excluded from figure 3.

To further quantify channel shape quality, we fabricated microfluidic valves (as described in figure 1) with the three methods that produced 10×100 μm channels (as well as with the control channels). With flow channel pressures of five and ten psi, we tested the necessary control channel pressure (up to a maximum of 25 psi) required to both slow and completely stop flow. The results of these tests are reported in table 1. While these tests were performed using air as the working fluid, we repeated the tests with water and found analogous results.

Table 1. Results of microfluidic valve testing with flow channels fabricated from the different methods that produced 10×100 μm channels.

	Flow pressure	Control pressure to slow flow	Control pressure to stop flow
Control	5 psi	13 psi	23 psi
	10 psi	19 psi	n/a
+PR	5 psi	11 psi	13 psi
	10 psi	15 psi	17 psi
3DP	5 psi	9 psi	12 psi
	10 psi	13 psi	17 psi
BSE	5 psi	4 psi	5 psi
	10 psi	10 psi	11 psi
IPM	—	—	—
SSC	—	—	—

Note: Control channels were 10×250 μm and the membrane thickness was approximately 50 μm. We report both the control pressure required to slow and completely stop flow, as determined by observing the rate of bubble production when we submerged tubing connected to the output of the flow channel. The maximum control pressure tested was 25 psi; above this value we classify the valve as exhibiting incomplete closure.

In figure 4, we plot the deviation of the actual dimensions from the target dimensions for all fabricated channels. For methods involving photolithography, the target dimensions are simply the dimensions of the photomask. For 3D printing, the target dimensions are the dimensions defined in the print file.

Control

As expected, control samples fabricated with SU-8 produced channels with nearly vertical sidewalls (see figure 3(a)). In fact, the sidewalls are slightly undercut (likely due to minor underexposure, despite using the manufacturer's recommended exposure energy), suggesting even worse valve closure performance. Compared to the target dimensions, the actual microchannels were consistently within just a few micrometers (for both channel width and channel height).

Reflow of positive photoresist

Determining an appropriate recipe for the positive photoresist we used (SPR 220-7.0) was extremely challenging (see supplemental information for full recipe details). In determining our recipe, we used the datasheet recipe as a starting point, but made modifications based on our equipment and other specifics. We found this process to be highly sensitive to small variations in procedure. Even more challenging was the variability of results from one experiment to the next, despite using the same process parameters. The source of this variability was likely do to the fact that fabrication was performed in a loosely regulated clean room, whereas processes that use this photoresist are typically performed in a much more tightly controlled cleanroom.

Once these challenges were overcome and we found a workable recipe, we were able to produce high quality microchannels in terms of both cross-sectional geometry and

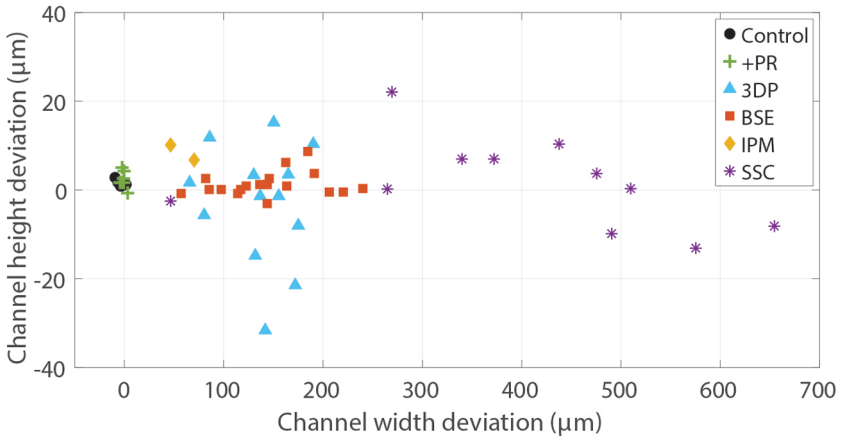

Figure 4. Plot showing the deviation of actual channel dimensions from those of the photomask (or, in the case of 3D printing, the print file). Each plotted point represents a distinct microchannel that was fabricated and measured.

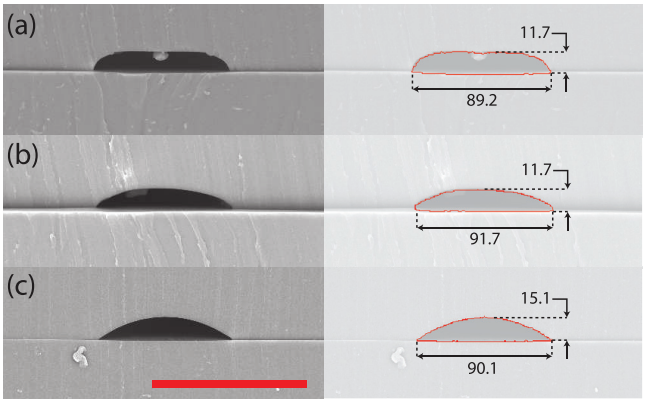

Figure 5. SEM images of 10×100 μm channels reflowed for five minutes at (a) 90 °C, (b) 120 °C, and (c) 150 °C. (Left) original SEM image. (Right) SEM image with channel highlighted and dimensions added. All dimensions are in micrometers. Scale bar is 100 μm.

resolution. As can be seen in figure 5, reflowing the post-development device at different temperatures allows for fine control of channel geometry. However, we were unable to achieve channels of 50 μm thickness, due to the complications introduced by attempting multiple spin coating steps, as noted previously (see the methods section). As has been noted by others [18], the final geometry of the microchannel is dependent on the processing parameters, and predicting the geometry of the final, rounded channels from the geometry of the rectangular channels is not as trivial as may be naively assumed.

In summary, this technique is able to produce very fine channel sizes with good control over channel shape, but is inappropriate for thicker channels. Additionally, this method requires strict process control and substantial infrastructure, which may make it inaccessible for many potential users.

3D printing

In general, the chosen 3D printers performed well; the cross section shape of the microchannels were all suitable. Using 3D printing for microfluidic valves is promising in that rounded

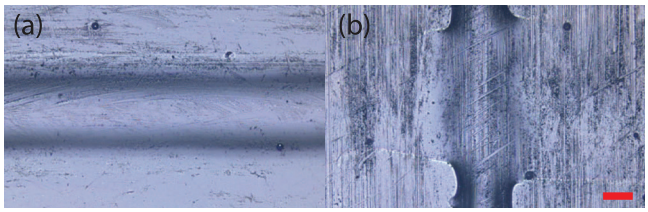

Figure 6. Confocal microscope images of channels printed (a) parallel and (b) perpendicular to the direction of travel of the print head of the Objet30 Scholar from Stratasys. In these images, the print head travels from left to right. Note how the microchannel in (a) is smooth and consistant while the microchannel in (b) is broken. Scale bar is 100 μm.

microchannels are achieved 'for free' at smaller dimensions due to either surface tension effects (in the case of the Objet30 and other Polyjet printers) or due to the spatial energy distribution of UV light projections (in the case of SLA printers like the Form 1+ and the Titan 1). Additionally, the fabrication process is extremely simple and almost entirely 'hands off'.

However, there are shortcomings. The resolution on current 3D printers is limited; many are unable to print at the size scale of interest, and those that are able can only do so at the expense of distorted dimensions. As can be seen in figure 3(c), there is poor correlation between the dimensions defined in the print file and the actual microchannels that are fabricated. However, if the relationship between the file dimensions and the physical dimensions is well understood, this problem can be avoided.

When printing on the Objet30, we were careful to control for print direction. One can see in figure 6 that the direction of travel of the print head has a substantial effect on the print quality of channels of these sizes. Ideally, one would always be able to align the direction of the channel with direction of travel of the print head. However, for most microfluidic chips this restriction is not feasible. For this reason, other printing technologies may be more appropriate.

As mentioned above, many printers are unable to print at the small scale in which we are interested. Even with the printers we examined here, we often tried to print below the advertised resolution, as can be see in table 2. When printing below the nominal resolution of the printer, we consistently found that feature dimensions were of compromised fidelity.

Table 2. Comparison of the advertised resolution for each printer used, from the corresponding manufacturer website.

	Feature size (μm)	Layer thickness (μm)
Objet30	100	28
Form 1+	300	25
Titan 1	50	5

Note: The 'feature size' corresponds to the XY resolution, while the 'layer thickness' corresponds to the Z resolution.

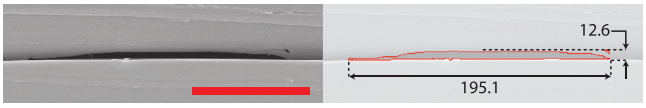

Figure 7. SEM image of 10×100 μm channel exposed at 175 mJ cm^{-2}. Notice the tearing in the top right of the channel. (Left) original SEM image. (Right) SEM image with channel highlighted and dimensions added. All dimensions are in micrometers. Scale bar is 100 μm.

We found that the Objet30 was unable to print the 50 μm wide channels at all.

Another relevant consideration is the tray size of the printer. Most high resolution printers have a limited build volume which is defined in part by the size of the build tray. While for many microfluidic applications this may not be an issue, it is a limitation that should be noted.

Finally, users may see limitations due to the surface roughness of the printed molds. As the printers in this study all employ printing styles (PolyJet, SLA, DLP SLA) that require thermosets, there are unfortunately few post-processing options that are viable, given the feature sizes of interest. In other types of printing (such as FDM) that use thermoplastics, parts may be treated with an acetone vapor polish to increase surface smoothness. If surface roughness becomes a significant issue, one solution is to simply use a more advanced printer. At the time of this writing, there are a number of high resolution DLP SLA printers that offer excellent surface quality; perhaps the highest surface quality is offered by printers using continuous liquid interface production (CLIP) [47].

In summary, 3D printing is an extremely simple method to produce rounded microchannels of good cross-sectional geometry. However, resolution is often limited, physical dimensions may vary greatly compared to print file dimensions, and overall print size can be small.

Backside exposure through glass wafer

As noted in the methods section, we used exposure energies that were either recommended by the photoresist datasheet, or slightly above. Comparatively higher exposure energies were reported by Futai *et al* [17]. Regardless, we found that increased exposure energy led to increased channel widths, in concurrence with Futai *et al*.

However, we did find some degree of tearing of the PDMS upon removal from the wafer. This phenomenon can be seen in figure 7. The tearing appears to have no correlation with channel dimension, as it was seen in different samples across

Figure 8. SEM image of 50×50 μm channel exposed at 150 mJ cm^{-2}. Notice the sharp corners at the top of the channel. (Left) original SEM image. (Right) SEM image with channel highlighted and dimensions added. All dimensions are in micrometers. Scale bar is 100 μm.

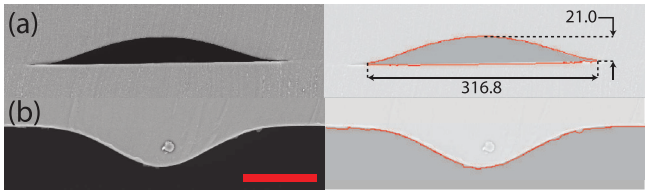

Figure 9. SEM images of 250 μm wide channels inflated at 5 psi. (a) 10 μm mold produced normal channels. (b) 50 μm mold produced collapsed channels. Consequently, this image does not include a bottom layer of PDMS. (Left) original SEM image. (Right) SEM image with channel highlighted and dimensions added. All dimensions are in micrometers. Scale bar is 100 μm.

a range of channel widths and heights (see also figure 8). Most likely, the relevant parameter here is the wafer material (all other wafers were silicon, whereas this technique requires glass). The authors are confident that this problem could be overcome with a simple surface treatment of the glass wafer.

While most channel shapes were similar to those shown in figure 3(d), some aspect ratio channels (most notably the narrow but tall channels, such as the 50×50 μm channels) showed sharp corners, as can be seen in figure 8. This effect may have to do with the specifics of the diffuser we used. Regardless, this technique may not be appropriate for taller channels.

In summary, this method provides a very simple fabrication process that is nearly as easy as standard photolithography with a silicon wafer. However, there is significant channel widening, and glass wafers typically cost about an order of magnitude more than silicon wafers.

Inflated PDMS membrane

When successful, this method produced satisfactory microchannels; however, the method quite often failed to produce channels at all. In contrast to Hongbin *et al* [21], we found little to no effect from increasing the pressure of the inflated membrane. This discrepancy may be due to the thickness of the inflated membrane. Hongbin *et al* report a membrane of about 20 μm from spincoating at 1000 rpm, but in our attempts spinning at 1000 rpm created membranes of much greater thickness (approximately 75 μm). With a thicker membrane, we would require much larger variations in pressure to see noticeable changes in deflection. While experimenting with higher pressures, we occasionally plastically deformed the thin membrane, revealing one failure mode of this technique.

We additionally tried spincoating at higher speeds to achieve thinner membranes (2000 rpm to fabricate an approximately 40 μm thick membrane), but encountered other

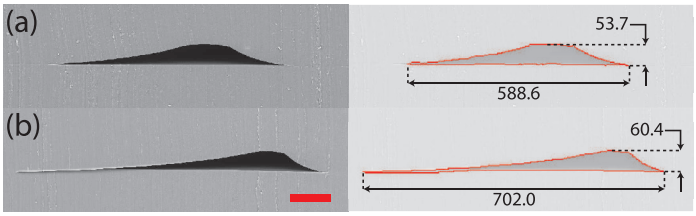

Figure 10. 50 μm tall channels with a secondary spin coating at 4000 rpm. (a) 100 μm wide channel (nominally), near the center of the wafer. (b) 250 μm wide channel (nominally), offset from the center of the wafer. Notice the increasing assymmetry with distance from the center of the wafer. (Left) original SEM image. (Right) SEM image with channel highlighted and dimensions added. All dimensions are in micrometers. Scale bar is 100 μm.

Table 3. Performance of the different fabrication strategies for different evaluation parameters.

	Evaluation parameter					
Fabrication strategy		Channel shape	Resolution	Dimension mapping	Fabrication time	Fabrication difficulty	Process prohibitiveness
	Control	×	11 μm (height) 60 μm (width)	2 μm (height) −4 μm (width)	45 min (active) 7 hr (total)	Moderate	Moderate
	+PR	✓	12 μm (height) 36 μm (width)	2 μm (height) −1 μm (width)	85 min (active) 11.5 hr (total)	Difficult	High
	3DP	✓	12 μm (height) 116 μm (width)	−3 μm (height) 137 μm (width)	30 min (active) 9 hr (total)	Easy	Low
	BSE	✓	9 μm (height) 119 μm (width)	1 μm (height) 145 μm (width)	45 min (active) 7 hr (total)	Moderate	Moderate
	IPM	✓	17 μm (height) 311 μm (width)	8 μm (height) 58 μm (width)	90 min (active) 17.5 hr (total)	Moderate	Moderate
	SSC	✓	10 μm (height) 327 μm (width)	2 μm (height) 403 μm (width)	55 min (active) 7 hr (total)	Moderate	Moderate

Note: Channel shape: a binary 'good' or 'bad' based on whether or not the given channel could be completely closed off when incorporated in a microfluidic valve. Resolution: these are the smallest widths and heights achieved when attempting to fabricate 10 × 50 μm channels (or the smallest successfully fabricated channel), rounded to the nearest micrometer. Dimension mapping: values obtained by averaging width and height deviation from the photomask or print file (as in figure 4) and rounding to the nearest micrometer. Fabrication time: we assume four hours for curing of PDMS and six hours for silanization of wafers and baking of 3D-printed molds (see supplemental information for more a detailed breakdown of fabrication time).

problems. With a thinner membrane, we noticed a tendency for the channels to collapse during curing. This effect is even more pronounced in wide, tall channels. In fact, we saw channel collapse in wide, tall channels even with the thicker membrane, as can be seen in figure 9.

As noted in the methods section, the channel height is partially a function of the channel width, so control over channel dimensions is limited. However, this relationship can be exploited as a benefit; one can create a single channel of varying height simply by varying the channel width.

In summary, this method is capable of producing channels of an appropriate shape, and has the interesting ability to create a single channel of variable height. However, the fabrication process involves many steps, is dependent on a variety of parameters, and is prone to frequent failure for more aggressive channel dimensions.

Secondary spin coating

Secondary spin coating is a very straightforward strategy to achieve rounded microchannels. We were unable to consistently achieve the 10 μm tall channels, as the secondary spin coating step effectively covered them. The 50 μm channels were all successfully fabricated, and produced channels with acceptable cross-sectional geometry.

However, there are two major drawbacks. First, the orientation and location of the microchannels with respect to the wafer are important. Channels aligned radially (i.e. whose long dimension passes through the wafer center) will be mostly symmetric, but those aligned tangentially will by asymmetric. The asymmetry increases with distance from the center of the wafer. This effect can be seen in figure 10.

The second drawback is a significant channel widening. It is typical for channel widths to grow hundreds of microns upon secondary spin coating. For example, the final width of the nominally 50 × 50 μm channel spun at 1000 rpm was over 600 μm. Note also that the height of the channels will change upon secondary spincoating, although this fact can be accounted for in the design.

In summary, this method is able to produce microchannels of the correct shape, but requires careful consideration of channel orientation, location, and spacing to create a functional microfluidic network.

Conclusions

As to which fabrication strategy is best for creating rounded microchannel, the answer is largely qualified; different strategies have different benefits and limitations. We have attempted to collect our findings in table 3, ranking each fabrication method on a number of metrics, which are described below.

It should be noted that all methods were able to produce channels of the appropriate shape, although to varying degrees. The quality of the channel shape is quantified by each channel's performance in a valve (see results section), but here we rank shape as a binary 'good' or 'bad' depending on whether or not there was complete channel closure. Resolution is quantified by the smallest channel heights and widths achieved when trying to fabricate 10×50 μm channels. If we were unable to fabricate 10×50 μm channels with a given method, we then used the smallest dimensions achieved in any successful channels. Specifically, all methods produced 10×50 μm channels except for the inflated PDMS membrane method, in which case we used the smallest dimensions from the 10×250 μm channels (as we were likewise unable to fabricate 10×100 μm channels). Dimension mapping is reported as an average deviation from target channel dimensions, as described in figure 4. Fabrication time lists both the active time (i.e. time that requires the user to be present) and the total time. We assume four hours for PDMS curing and six hours for wafer silanization and mold baking. Fabrication difficulty and process prohibitiveness are ranked qualitatively based on our experience with the various fabrication methods and the infrastructure, safety precautions, etc required.

In terms of ultimate resolution and dimension mapping, the reflow of positive photoresist performed best by far. However, this method has the drawbacks of a complicated fabrication process, high sensitivity to process parameters and disturbances, the use of dangerous chemicals, and the need for expensive infrastructure. On the other end of the spectrum is 3D printing. This method is extremely easy, fast, safe, and requires almost no user skill. However, resolution is limited, and channels often do not print at the dimensions specified in the design file.

The other methods each have their own strengths and weaknesses. Exposing through the backside of a glass wafer yields resolutions and controllability approaching that of reflowing positive photoresist, but allows one to work with much easier, safer, and more robust negative photoresists (such as SU-8). However, channel shape is not always ideal, there is significant channel widening, and glass wafers are significantly more expensive than silicon wafers. Using an inflated PDMS membrane as a mold enables the creation of individual channels with varying heights, but the fabrication process is long and inconsistent, and molds are somewhat fragile. Secondary spin coating is extremely simple and produces a very robust mold, but channel dimensions grow significantly and, unless the channels are placed very deliberately, the channels become asymmetric. We summarize the major factors affecting channel height, width, and degree of rounding in the supplemental information.

Acknowledgments

This work was supported by the Wyss Institute for Biologically Inspired Engineering, and the Army Research Office, National Defense Science and Engineering Graduate (NDSEG) Fellowship. Any opinions, findings, conclusions, or recommendations expressed in this material are those of the authors and do not necessarily reflect those of the funding organizations. The authors thank James C. Weaver for his assistance with the SEM images.

References

[1] Borenstein J T, Tupper M M, Mack P J, Weinberg E J, Khalil A S, Hsiao J and García-Cardeña G 2010 *Biomed. Microdevices* **12** 71–9
[2] Wong K H, Chan J M, Kamm R D and Tien J 2012 *Annu. Rev. Biomed. Eng.* **14** 205–30
[3] Emerson D R, Cieślicki K, Gu X and Barber R W 2006 *Lab Chip* **6** 447–54
[4] Psaltis D, Quake S R and Yang C 2006 *Nature* **442** 381–6
[5] Bellouard Y, Said A, Dugan M and Bado P 2004 *Opt. Express* **12** 2120–9
[6] Maselli V, Osellame R, Cerullo G, Ramponi R, Laporta P, Magagnin L and Cavallotti P L 2006 *Appl. Phys. Lett.* **88** 191107
[7] Unger M A, Chou H P, Thorsen T, Scherer A and Quake S R 2000 *Science* **288** 113–6
[8] Thorsen T, Maerkl S J and Quake S R 2002 *Science* **298** 580–4
[9] Chou H P, Unger M A and Quake S R 2001 *Biomed. Microdevices* **3** 323–30
[10] Liu J, Williams B A, Gwirtz R M, Wold B J and Quake S 2006 *Angew. Chem. Int. Ed.* **45** 3618–23
[11] Melin J and Quake S R 2007 *Annu. Rev. Biophys. Biomol. Struct.* **36** 213–31
[12] Fu A Y, Chou H P, Spence C, Arnold F H and Quake S R 2002 *Anal. Chem.* **74** 2451–7
[13] Wang Y C, Choi M H and Han J 2004 *Anal. Chem.* **76** 4426–31
[14] Hua Z, Xia Y, Srivannavit O, Rouillard J M, Zhou X, Gao X and Gulari E 2006 *J. Micromech. Microeng.* **16** 1433
[15] Devaraju N S G K and Unger M A 2012 *Lab Chip* **12** 4809–15
[16] Studer V, Hang G, Pandolfi A, Ortiz M, Anderson W F and Quake S R 2004 *J. Appl. Phys.* **95** 393–8
[17] Futai N, Gu W and Takayama S 2004 *Adv. Mater.* **16** 1320–3
[18] Fordyce P, Diaz-Botia C, DeRisi J and Gomez-Sjoberg R 2012 *Lab Chip* **12** 4287–95
[19] Kartalov E P, Scherer A, Quake S R, Taylor C R and Anderson W F 2007 *J. Appl. Phys.* **101** 064505
[20] Pandolfi A and Ortiz M 2006 *7th Int. Conf. on Thermal, Mechanical and Multiphysics Simulation and Experiments in Micro-Electronics and Micro-Systems* pp 1–4
[21] Hongbin Y, Guangya Z, Siong C F, Shouhua W and Feiwen L 2009 *Sensors Actuators* B **137** 754–61
[22] Rohde C B, Zeng F, Gonzalez-Rubio R, Angel M and Yanik M F 2007 *Proc. Natl Acad. Sci.* **104** 13891–5
[23] Wang G J, Ho K H, Hsu S H and Wang K P 2007 *Biomed. Microdevices* **9** 657–63
[24] Wang G J, Hsueh C C, Hsu S H and Hung H S 2007 *J. Micromech. Microeng.* **17** 2000
[25] Conradie E H and Moore D F 2002 *J. Micromech. Microeng.* **12** 368
[26] Abgrall P, Conedera V, Camon H, Gue A M and Nguyen N T 2007 *Electrophoresis* **28** 4539–51

[27] Dy A J, Cosmanescu A, Sluka J, Glazier J A, Stupack D and Amarie D 2014 *J. Micromech. Microeng.* **24** 057001
[28] McDonald J C, Chabinyc M L, Metallo S J, Anderson J R, Stroock A D and Whitesides G M 2002 *Anal. Chem.* **74** 1537–45
[29] Saggiomo V and Velders A H 2015 Simple 3D printed scaffold-removal method for the fabrication of intricate microfluidic devices *Adv. Sci.* **2**
[30] Waheed S, Canyelles J M C, Macdonald N, Guijt R M, Lewis T, Paull B and Breadmore M C 2016 3D printed microfluidic devices: enablers and barriers *Lab Chip* **16** 1993–2013
[31] Chen C, Hirdes D and Folch A 2003 *Proc. Natl Acad. Sci.* **100** 1499–504
[32] Wu H, Odom T W and Whitesides G M 2002 *Anal. Chem.* **74** 3267–73
[33] Lu Y and Chen S 2008 *Appl. Phys. Lett.* **92** 041109
[34] Zhou F, Cao W, Dong B, Reissman T, Zhang W and Sun C 2016 Additive manufacturing of a 3D terahertz gradient-refractive index lens *Adv. Opt. Mater.* **4** 1034–40
[35] Lee K, Kim C, Shin K S, Lee J W, Ju B K, Kim T S, Lee S K and Kang J Y 2007 *J. Micromech. Microeng.* **17** 1533
[36] Abdelgawad M, Wu C, Chien W Y, Geddie W R, Jewett M A and Sun Y 2011 *Lab Chip* **11** 545–51
[37] Tanaka H and Wood R J 2010 *J. Micromech. Microeng.* **20** 075008
[38] Song S H, Lee C K, Kim T J, Shin I C, Jun S C and Jung H I 2010 *Microfluid. Nanofluid.* **9** 533–40
[39] Jia Y, Jiang J, Ma X, Li Y, Huang H, Cai K, Cai S and Wu Y 2008 *Chin. Sci. Bull.* **53** 3928–36
[40] Asthana A, Kim K O, Perumal J, Kim D M and Kim D P 2009 *Lab Chip* **9** 1138–42
[41] Perry H, Greiner C, Georgakoudi I, Cronin-Golomb M and Omenetto F G 2007 *Rev. Sci. Instrum.* **78** 044302
[42] Verma M K, Majumder A and Ghatak A 2006 *Langmuir* **22** 10291–5
[43] Czaplewski D A, Kameoka J, Mathers R, Coates G W and Craighead H 2003 *Appl. Phys. Lett.* **83** 4836–8
[44] Qin D, Xia Y and Whitesides G M 2010 *Nat. Protocols* **5** 491–502
[45] Xia Y and Whitesides G M 1998 *Annu. Rev. Mater. Sci.* **28** 153–84
[46] Koukharenko E, Kraft M, Ensell G and Hollinshead N 2005 *J. Mater. Sci.: Mater. Electron.* **16** 741–7
[47] Tumbleston J R *et al* 2015 *Science* **347** 1349–52